

Experimental investigation of the large amplitude vibrations of a thin-walled column under self-weight

Paulo B. Gonçalves^{*1}, Daniel Leonardo B.R. Jurjo^{2a}, Carlos Magluta^{2b} and Ney Roitman^{2b}

¹Department of Civil Engineering, Catholic University, PUC-Rio, 22453-900, Rio de Janeiro, RJ, Brazil

²Department of Civil Engineering, Federal University of Rio de Janeiro, COPPE/UFRJ, Rio de Janeiro, RJ, Brazil

(Received March 27, 2012, Revised April 17, 2013, Accepted May 31, 2013)

Abstract. This work presents an experimental methodology specially developed for the nonlinear large-amplitude free vibration analysis of a clamped-free thin-walled metal column under self-weight. The main contribution of this paper is related to the developed experimental methodology which is based on a remote sensing technique using a computer vision system that integrates, on-line, the digital image acquisition and its treatment through special image processing routines. The main importance of this methodology is that it performs large deflections measurements without making contact with the structure and thus, not introducing undesirable changes in its behavior, for instance, appreciable changes in mass and stiffness properties. This structure presents, in most cases, highly non-linear responses, which cannot be reproduced by conventional finite-element softwares due, mainly, to the simultaneous influence of geometric and inertial non-linearities. To capture the non-linearities associated with large amplitude vibration and be able to describe the buckling process, the structure is discretized as a sequence of jointed coupled elastic pendulums. The obtained numerical results are favorably compared with the experimental ones, in the pre- and post-buckling regimes.

Keywords: nonlinear vibrations; large deflection behavior; softening phenomenon; dynamic experimental analysis; digital image processing; non-contact displacement measurements

1. Introduction

As structures become lighter and thinner, the non-linear effects become increasingly important and difficult to be controlled. The catastrophic collapse of several large structures or the unexpected behavior of certain structures, requiring costly changes in project, reinforcement, or the use of control systems, demonstrate this fact. Therefore, the static and dynamic analysis of non-linear structural systems presents to engineers and researchers a variety of difficult problems to solve. The influence of the self-weight on the buckling and non-linear dynamic behavior of uni-dimensional slender structures has been a subject of considerable interest in recent years, mainly

*Corresponding author, Professor, E-mail: paulo@puc-rio.br

^aD.Sc.

^bProfessor

due to the increasing slenderness of the structural elements. This is also a topic of relevance in non-linear mechanics, as shown by the following recent contributions and their references. Virgin and Plaut (2004) investigated the post-buckling behavior and vibration frequencies of linearly elastic and softening columns under self-weight. The governing equations were solved numerically with the use of a shooting method and experiments were conducted to verify the results qualitatively. Vaz and Mascaro (2005) analyzed the post-buckling behavior of slender elastic vertical rods subjected to terminal forces and self-weight. A perturbation method was used to find the critical buckling loads and initial post-buckling solutions and a numerical integration scheme based on the shooting method was employed in the post-buckling solutions. Gonçalves *et al.* (2006) studied the buckling and post-buckling behavior of slender bars under self-weight, including the influence of boundary conditions on the stability and large deflection behavior of the bar. Santillan *et al.* (2008) studied the large-amplitude first-mode vibration of a cantilever with non-zero self-weight using numerical simulations and a perturbation analysis. Sadiku (2008) discussed the problem of achieving the weight distribution of a column, along its height, that optimizes the buckling load of the column, taking into consideration the column self-weight. Duan and Wang (2008) derived an exact solution for the buckling of columns including self-weight while Wang (2010) investigated the vibrations of a segmented heavy column. Tolou and Herder (2009) developed a semi analytical approach to study the large deflections of compliant beams under point load. Jurjo *et al.* (2010) presented an experimental methodology for the analysis of slender structures based on digital image processing technique. Wei *et al.* (2010) determined the critical load for non-prismatic columns under self-weight and tip force. Neukirch *et al.* (2012) studied the small-amplitude in-plane vibrations of an elastic rod in the post-buckling regime. The vibration frequencies were computed both analytically and numerically as a function of the loading.

In the present work, the thin-walled column is modeled as a system of multiple pendulums (Galán *et al.* 2005, Jurjo 2007). This model aims to represent accurately the large rotations which take place during the column vibration, particularly for column longer than the critical buckling length under self-weight (L_{cr}), as well as the geometric and inertial nonlinearities which play an important role in the nonlinear vibrations of long columns (Chirikov 2005, Nayfeh and Pai 2004, Sathyamoorthy 1998). The resulting Euler-Lagrange equations of motion are solved by the fourth order Runge-Kutta numerical method. In their book Nayfeh and Pai (2004) present some alternative formulations as well as analytical, numerical and experimental results on the planar and non-planar nonlinear vibrations of slender columns including geometric and inertial nonlinearities.

To evaluate the efficiency and accuracy of the numerical methodology in obtaining the nonlinear dynamic responses, an experimental methodology has also been developed, based on digital image processing techniques (Hack and Leroy 2005, Yoneyama *et al.* 2005, Lee and Shinozuka 2006a, b, Jones *et al.* 2006, Jurjo *et al.* 2010). These techniques are rapidly developing, mainly due to the progresses obtained in image acquisition systems and in the development of computers, algorithms and softwares used for general or specific applications.

The importance of this experimental methodology is that it enables one to perform non-contact displacement measurements without introducing undesirable changes in the structure's behavior, since the presence of conventional contact sensors may cause changes in its behavior due to the extreme flexibility (high index of slenderness) of the structure. Taking this into consideration, the proposed experimental methodology only uses adhesive markers of a negligible mass compared to that of the structure (Jurjo 2007). This methodology can also be applied to large civil engineering structures, such as bridges and viaducts, where the access for the installation of the conventional instrumentation is usually rather difficult (Lee and Shinozuka 2006a, b). This is also a promising

technique for structures under finite deformations (Jones *et al.* 2006).

This experimental methodology has been used in an online computer-based vision system, which integrates acquisition and data processing of the images through special programming routines, which make it possible to sharpen the image, identify the adhesive markers (points of interest) and extract their coordinates in the image and convert them to engineering units. Taking image as a movement sensor, several experiments have been undertaken using a clamped-free thin-walled metal column under self-weight in the pre- and post-buckling regimes with different lengths, so that is possible to analyze its non-linear dynamic behavior in these conditions. The comparison between numerical and experimental results shows that the present experimental methodology is easy to implement and leads to a precise description of the highly non-linear response of the slender column under self-weight.

2. Equations of motion and computational implementation

In the present work, the thin-walled column is modeled as a chain of n elastically jointed pendulums, as shown in Fig. 1. The nonlinear equations of motion are here obtained by Hamilton's principle. The Lagrange's function is given by

$$L_f = T - \Pi_p \tag{1}$$

where T and Π_p are, respectively, the kinetic and total potential energy of the structure. The kinetic energy is a function of the generalized coordinates and generalized velocities, while the total potential energy is a function of generalized coordinates only.

The structure's total potential energy is given by

$$\Pi_p = U + V \tag{2}$$

where U and V are, respectively, the internal strain energy and the potential energy of the applied load.

Considering that the column is modeled as a sequence of n coupled pendulums connected by damped rotational springs, the kinetic and potential energies can be written as (Braun 2003, Galán *et al.* 2005, Jurjo 2007)

$$T_k = \frac{1}{2} m_k \sum_{i=1}^k \sum_{j=1}^k l_i l_j \dot{\theta}_i \dot{\theta}_j \cos(\theta_i - \theta_j) \tag{3}$$

$$V_k = m_k g \sum_{i=1}^k l_i (1 - \cos \theta_i) \tag{4}$$

where m_k , g and l_i are, respectively, mass, gravity acceleration and pendulum length, and θ_i and

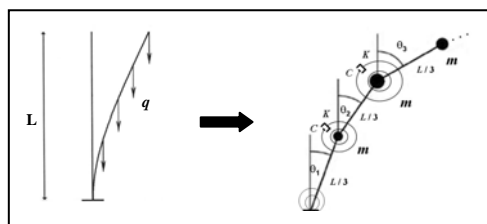


Fig. 1 Column modeling as a sequence of coupled pendulums

$\dot{\theta}_i$ are the generalized coordinates and velocities. Here the column is discretized as n pendulums with the same mass and stiffness (Galán *et al.* 2005).

Each joint (including the bottom support point) is assumed to have a rotational stiffness K which contributes to the elastic potential energy, being unstressed when each pendulum points vertically. Thus, the strain energy associated to the springs' rotations is given by

$$U = \frac{1}{2} K \theta_1^2 + \frac{1}{2} K \left[\sum_{i=1}^k (\theta_{i+1} - \theta_i)^2 \right] \tag{5}$$

From Eqs. (1), (3), (4) and (5), the energy functional for a sequence of n coupled pendulums is given by

$$L_f = \sum_{k=1}^n \left\{ \left[\frac{1}{2} m_k \sum_{i=i}^k \sum_{j=1}^k l_i l_j \dot{\theta}_i \dot{\theta}_j \cos(\theta_i - \theta_j) \right] - \left[\frac{1}{2} K \theta_1^2 + \frac{1}{2} K \sum_{i=1}^k (\theta_{i+1} - \theta_i)^2 \right] - \left[m_k g \sum_{i=1}^k l_i (1 - \cos \theta_i) \right] \right\} \tag{6}$$

The Euler-Lagrange equations of motion are

$$\frac{\partial L}{\partial \theta_i} - \frac{d}{dt} \left(\frac{\partial L}{\partial \dot{\theta}_i} \right) = Q_i, \quad i = 1, 2, \dots, n \tag{7}$$

where Q_i are the non-conservative generalized forces, including damping forces. The damping is modeled by means of a Rayleigh dissipation function. Each joint is supposed to experience a damping force $C(\theta_{i+1} - \theta_i)$ proportional to the angular velocity of the joint.

Thus, the equations of motion can be written in matrix form as

$$\begin{aligned} & \begin{bmatrix} \sum_{i=1}^n m_i l^2 & \sum_{i=2}^n m_i l^2 \cos(\theta_1 - \theta_2) & \sum_{i=3}^n m_i l^2 \cos(\theta_1 - \theta_3) & \sum_{i=4}^n m_i l^2 \cos(\theta_1 - \theta_4) \\ \sum_{i=2}^n m_i l^2 \cos(\theta_1 - \theta_2) & \sum_{i=2}^n m_i l^2 & \sum_{i=3}^n m_i l^2 \cos(\theta_2 - \theta_3) & \sum_{i=4}^n m_i l^2 \cos(\theta_2 - \theta_4) \\ \sum_{i=3}^n m_i l^2 \cos(\theta_1 - \theta_3) & \sum_{i=3}^n m_i l^2 \cos(\theta_2 - \theta_3) & \sum_{i=3}^n m_i l^2 & \sum_{i=4}^n m_i l^2 \cos(\theta_3 - \theta_4) \\ \sum_{i=4}^n m_i l^2 \cos(\theta_1 - \theta_4) & \sum_{i=4}^n m_i l^2 \cos(\theta_2 - \theta_4) & \sum_{i=4}^n m_i l^2 \cos(\theta_3 - \theta_4) & \sum_{i=4}^n m_i l^2 \end{bmatrix} \begin{bmatrix} \ddot{\theta}_1 \\ \ddot{\theta}_2 \\ \ddot{\theta}_3 \\ \ddot{\theta}_4 \\ \vdots \end{bmatrix} + \\ & \begin{bmatrix} 0 & \sum_{i=2}^n m_i l^2 \sin(\theta_1 - \theta_2) & \sum_{i=3}^n m_i l^2 \sin(\theta_1 - \theta_3) & \sum_{i=4}^n m_i l^2 \sin(\theta_1 - \theta_4) \\ -\sum_{i=2}^n m_i l^2 \sin(\theta_1 - \theta_2) & 0 & \sum_{i=3}^n m_i l^2 \sin(\theta_2 - \theta_3) & \sum_{i=4}^n m_i l^2 \sin(\theta_2 - \theta_4) \\ -\sum_{i=3}^n m_i l^2 \sin(\theta_1 - \theta_3) & -\sum_{i=3}^n m_i l^2 \sin(\theta_2 - \theta_3) & 0 & \sum_{i=4}^n m_i l^2 \sin(\theta_3 - \theta_4) \\ -\sum_{i=4}^n m_i l^2 \sin(\theta_1 - \theta_4) & -\sum_{i=4}^n m_i l^2 \sin(\theta_2 - \theta_4) & -\sum_{i=4}^n m_i l^2 \sin(\theta_3 - \theta_4) & 0 \end{bmatrix} \begin{bmatrix} \dot{\theta}_1^2 \\ \dot{\theta}_2^2 \\ \dot{\theta}_3^2 \\ \dot{\theta}_4^2 \\ \vdots \end{bmatrix} + \\ & \begin{bmatrix} \sum_{i=1}^n g l m_i & 0 & 0 & 0 \\ 0 & \sum_{i=2}^n g l m_i & 0 & 0 \\ 0 & 0 & \sum_{i=3}^n g l m_i & 0 \\ 0 & 0 & 0 & \sum_{i=4}^n g l m_i \end{bmatrix} \begin{bmatrix} \sin \theta_1 \\ \sin \theta_2 \\ \sin \theta_3 \\ \sin \theta_4 \\ \vdots \end{bmatrix} + \\ & \begin{bmatrix} 2K & -K & 0 & 0 \\ -K & 2K & -K & 0 \\ 0 & -K & 2K & -K \\ 0 & 0 & -K & K \end{bmatrix} \begin{bmatrix} \theta_1 \\ \theta_2 \\ \theta_3 \\ \theta_4 \\ \vdots \end{bmatrix} + \begin{bmatrix} 2C & -C & 0 & 0 \\ -C & 2C & -C & 0 \\ 0 & -C & 2C & -C \\ 0 & 0 & -C & C \end{bmatrix} \begin{bmatrix} \dot{\theta}_1 \\ \dot{\theta}_2 \\ \dot{\theta}_3 \\ \dot{\theta}_4 \\ \vdots \end{bmatrix} = \begin{bmatrix} 0 \\ 0 \\ 0 \\ 0 \\ \vdots \end{bmatrix} \tag{8} \end{aligned}$$

where $\ddot{\theta}$ and C are, respectively, the angular acceleration and the damping coefficient, or, in a more compact form

$$RM.\ddot{\theta} + RJ.\dot{\theta}^2 + RW.\sin\theta + RK.\theta + RC.\dot{\theta} = 0 \quad (9)$$

where RM , RJ , RW , RK and RC are, respectively, mass, gyroscopic (anti-symmetrical), gravitational potential, stiffness and damping matrices. So, the present formulation takes into account in full the inertial and geometric nonlinearities associated with the large displacements and rotations of the column, being capable of describing its large amplitude vibrations and post-buckling configurations.

3. Experimental methodology (Computer Based-Vision System)

The experimental methodology encompasses the following steps:

(i) Digitalization: the analogical images captured by the video camera are converted into digital images through a monochromatic digitalization board; **(ii) Digital image processing:** the quality of the acquired image is enhanced to provide a better identification of the coordinates (u, v) of the centroids of the points of interest. **(iii) Calibration:** the purpose of this step is to determine the transformation matrix that correlates the image and their respective actual coordinates. To obtain the coordinates transformation matrix it is necessary to apply an adequate calibration method. In this study the DLT method is used (Abdel-Aziz and Karara 1971); **(iv) Reconstruction:** This step consists in obtaining the actual coordinates by using the transformation matrix and the image coordinates.

From these steps, a computational vision system, based on the programming language LabVIEW, which deals with, in real time, the acquisition and the processing of the digital image is developed. The camera used in this study has analogical video signals. The image capture mode is based on a non-interlinked analogical video signal, denominated field. In this mode, the image is composed of a single field, even or odd, with a time interval between them of 1/60s. The field mode results in an image with half of the height, and twice the capture frequency of the frame mode (30 frames/second), i.e., 60 frames/second.

3.1 Image-sensor program

The processing routine of the Image-Sensor Program (ISP) consists in: (i) the definition of the area of interest of the image under analysis, enabling the reduction of the processing time and interference of objects that are outside this area. (ii) The definition of the threshold of the transformation of gray tone images (8 bits) into binary ones (one bit, where 0 is black and 1 is white), highlighting the points of interest and eliminating the remaining interferences in the image. (iii) The identification of the points of interest, enabling the calculation of the image coordinates u and v of the centroids of these points.

The calculation of the u and v coordinates of the points of interest highlighted in the image is achieved by transforming these points into small regions known in image processing as ROI (regions of interest). A ROI is characterized by a record (set of data) which contains the coordinates of the contour of a region of interest.

The points of interest can be converted into ROIs by putting a “mask” over the binarized

image. In this image, only the points of interest are white, while the background is black. In this way, the mask can identify each one of the regions, searching the (u, v) coordinates of the borders between the white and black pixels. In possession of the borders coordinates, it is possible to determine the centroids of each of the regions of interest.

The ISP was developed in such a way that the acquisition and processing routines are executed in parallel. So, while the acquisition routine waits and digitalizes an analogical image, the processing one segments (binarizes), identifies and calculates the coordinates of the image points of interest, highlighted in the last digitalized image. After this, the ISP search routine selects, within the set of identified points of interest, those whose motion is desired. These points are called analysis points. The advantage of this part of the program is that the search routines are part of a post-processing scheme, which is independent of the image processing routine. Consequently, it results in a faster processing routine.

From the developed search methods, which are part of the search routine, it is possible to obtain the image coordinates (u, v) of the points of analysis along every frame acquired during a certain period.

The calibration is performed by identifying the (u, v) coordinates of the calibration points selected in the image and inserting the respective actual coordinates (x, y) (2D) or (x, y, z) (3D). This step is carried out by the calibration routine.

In order to obtain the coordinates transformation matrix, which establishes the correlation between the actual coordinates and the ones in the image, it is necessary to apply an adequate calibration method. Among the several existing calibration methods, the most common is the DLT (Direct Linear Transformation) (Abdel-Aziz and Karara 1971, Hatze 1988, Chen *et al.* 1994, Tsai 1986, Faugeras and Toscani 1986, Ito 1991, Weng *et al.* 1992). The standard DLT is chosen here due to the low level of distortions caused by the video camera lenses.

From the data collected in the calibration routine and with the use of the DLT method, ISP determines the coordinate transformation matrix. Through this matrix, and using the u and v image coordinates determined for each one of the points of analysis, ISP obtains the respective actual coordinates.

3.2 DLT method

Using the DLT method (Haralick and Shapiro 1993), the relation between the image coordinates (u, v) and its respective actual ones (x, y) in the plane, is given by

$$\begin{aligned} xL_1 + yL_2 + L_3 - uxL_7 - vyL_8 &= u \\ xL_4 + yL_5 + L_6 - vxL_7 - vyL_8 &= v \end{aligned} \quad (10)$$

where the coefficients L_i are the calibration **DLT parameters**.

Since the number of unknowns in Eq. (10) is equal to eight (DLT parameters), at least 4 points are necessary to calculate the coefficients L_i . Taking n reference points, the following system is obtained.

$$\begin{bmatrix} x_1 & y_1 & 1 & 0 & 0 & 0 & -u_1x_1 & u_1y_1 \\ 0 & 0 & 0 & x_1 & y_1 & 1 & -v_1x_1 & -v_1y_1 \\ & & & & \vdots & & & \\ x_n & y_n & 1 & 0 & 0 & 0 & -u_nx_n & -u_ny_n \\ 0 & 0 & 0 & x_n & y_n & 1 & -v_nx_n & -v_ny_n \end{bmatrix} \begin{bmatrix} L_1 \\ L_2 \\ \vdots \\ L_7 \\ L_8 \end{bmatrix} = \begin{bmatrix} u_1 \\ v_1 \\ \vdots \\ u_n \\ v_n \end{bmatrix} \quad (11)$$

If $n > 4$, the system cannot be directly solved, since it is over-determined. In this case, the problem can be solved using the Least Square Method (LSM), which will search for the best adjustment of the “ L_i ” coefficients from the set of actual and image coordinates, minimizing the errors. The application of the LSM to Eq. (11) can be represented as

$$A_{2n \times 8} \cdot L_{8 \times 1} = B_{2n \times 1} \tag{12}$$

Multiplying both sides of Eq. (12) by the transposed of matrix A will result in

$$C_{8 \times 8} \cdot L_{8 \times 1} = D_{8 \times 1} \tag{13}$$

Manipulating Eq. (10) in order to make (x, y) explicit, the following equation is obtained

$$\begin{bmatrix} L_1^{(1)} - u^{(1)}L_7^{(1)} & L_2^{(1)} - u^{(1)}L_8^{(1)} \\ L_4^{(1)} - v^{(1)}L_7^{(1)} & L_5^{(1)} - v^{(1)}L_8^{(1)} \end{bmatrix} \begin{bmatrix} x \\ y \end{bmatrix} = \begin{bmatrix} u^{(1)} - L_3^{(1)} \\ v^{(1)} - L_6^{(1)} \end{bmatrix} \tag{14}$$

In order to minimize errors in the values of the (x, y) coordinates, this process can be extended to m cameras, through the equations

$$\begin{bmatrix} L_1^{(1)} - u^{(1)}L_7^{(1)} & L_2^{(1)} - u^{(1)}L_8^{(1)} \\ L_4^{(1)} - v^{(1)}L_7^{(1)} & L_5^{(1)} - v^{(1)}L_8^{(1)} \\ \vdots & \vdots \\ L_1^{(m)} - u^{(m)}L_7^{(m)} & L_2^{(m)} - u^{(m)}L_8^{(m)} \\ L_4^{(m)} - v^{(m)}L_7^{(m)} & L_5^{(m)} - v^{(m)}L_8^{(m)} \end{bmatrix} \begin{bmatrix} x \\ y \end{bmatrix} = \begin{bmatrix} u^{(1)} - L_3^{(1)} \\ v^{(1)} - L_6^{(1)} \\ \vdots \\ u^{(m)} - L_3^{(m)} \\ v^{(m)} - L_6^{(m)} \end{bmatrix} \tag{15}$$

where m is the number of cameras.

Eq. (15) results in an over-determined system, which can again be solved by applying the LSM

$$E_{2 \times 2m}^T E_{2 \times 2m} \cdot R_{2 \times 1} = E_{2 \times 2m}^T F_{2 \times 1} \tag{16}$$

Once the (u, v) coordinates of the image of the same point in several cameras (at least two cameras) and the “ L ” coefficients of each one of the cameras are known, their actual coordinates (x, y) can be obtained through the Eq. (16).

3.3 Experimental apparatus

The apparatus used to perform the experimental analysis is presented in Fig. 2 and consists of the column, the video camera, the non-oscillating illumination system and the adhesive markers. A special clamp for the column was designed to enable the variation of the column length during the experiments. A metallic sheet of brass representing a slender column with width $b = 9.0$ cm; thickness $h = 0.45$ mm; load per unit length (self-weight) $q = 3.43$ N/m; Young’s Modulus $E = 123257$ MPa (mean values of the experimental results) and critical length (L_{cr}): 56.44, is used in the experiments. The tests were performed with different column lengths, longer (60, 70 cm) and shorter (30, 40, 50 cm) than the critical buckling length (L_{cr}), enabling an analysis of the dynamic behavior along the fundamental and post-critical equilibrium paths.

In this study, a black background was used to minimize interferences verified in images acquired with the use of other background colors (Jurjo 2007). The advantages of the black background are to facilitate the image processing and, particularly, eliminate shadows generated

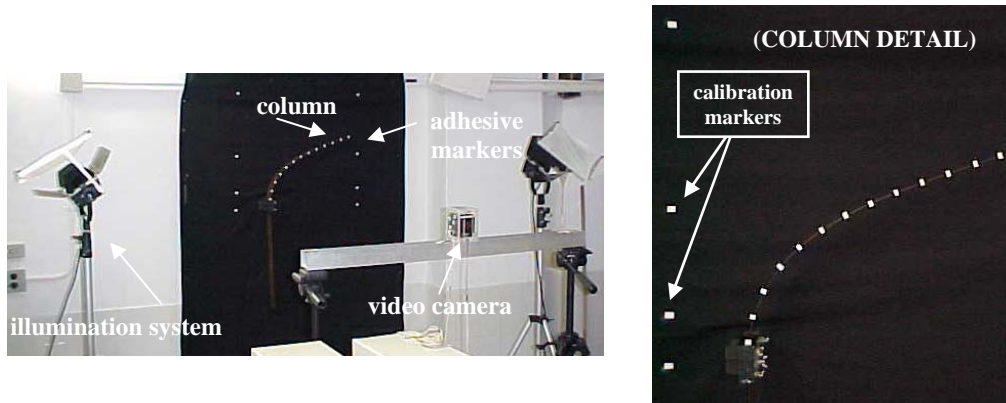


Fig. 2 Apparatus used in the experimental analysis

by the column on the background.

To represent the points of interest, small white rectangular adhesives markers are used. These adhesives are placed along the length of the column at pre-established distances, to obtain the displacements and the deformed shapes of the column at different instants of time. These markers were also placed on the black background, in order to help in the calibration process. Fig. 2 shows the disposition of the points of interest in the columns and in the calibration.

To analyze the free vibration responses, the following strategy was adopted: columns with a length smaller than the critical one are subjected to an initial displacement (and null velocity); on the other hand, columns with a length greater than the critical one are released from the vertical unstable equilibrium position. In this case, the column diverges initially from the unstable configuration, presenting a sharp downward movement and, after this, vibrates around the stable post-buckling configuration. For the tensioned configuration, since this configuration is always stable, an initial displacement is imposed to the free end of the column.

As mentioned previously, only one video camera is used with image capture in the field mode. Despite introducing more imprecision in the analysis, this has the advantage of a higher capture frequency (60 frames/s). This frequency is essential in the analysis of columns with lengths above the critical value, mainly in the first instants, when the column, during the process of divergence from the unstable equilibrium position, exhibits large displacements and velocities.

With the use of ISP, the time responses of the x and y coordinates of the markers placed along the column is obtained for all of the analyzed configurations. In this way, it is possible to determine the natural frequencies and damping rates for the different column lengths.

4. Results and comments

First a convergence analysis is carried out to define the discretization of the column as a multiple pendulum. Fig. 3 presents the variation of the natural frequency as a function of the number of pendulums, for different columns lengths under compression ($L < L_{cr}$ and $L > L_{cr}$). These results are obtained through the resolution of the eigenvalue problem

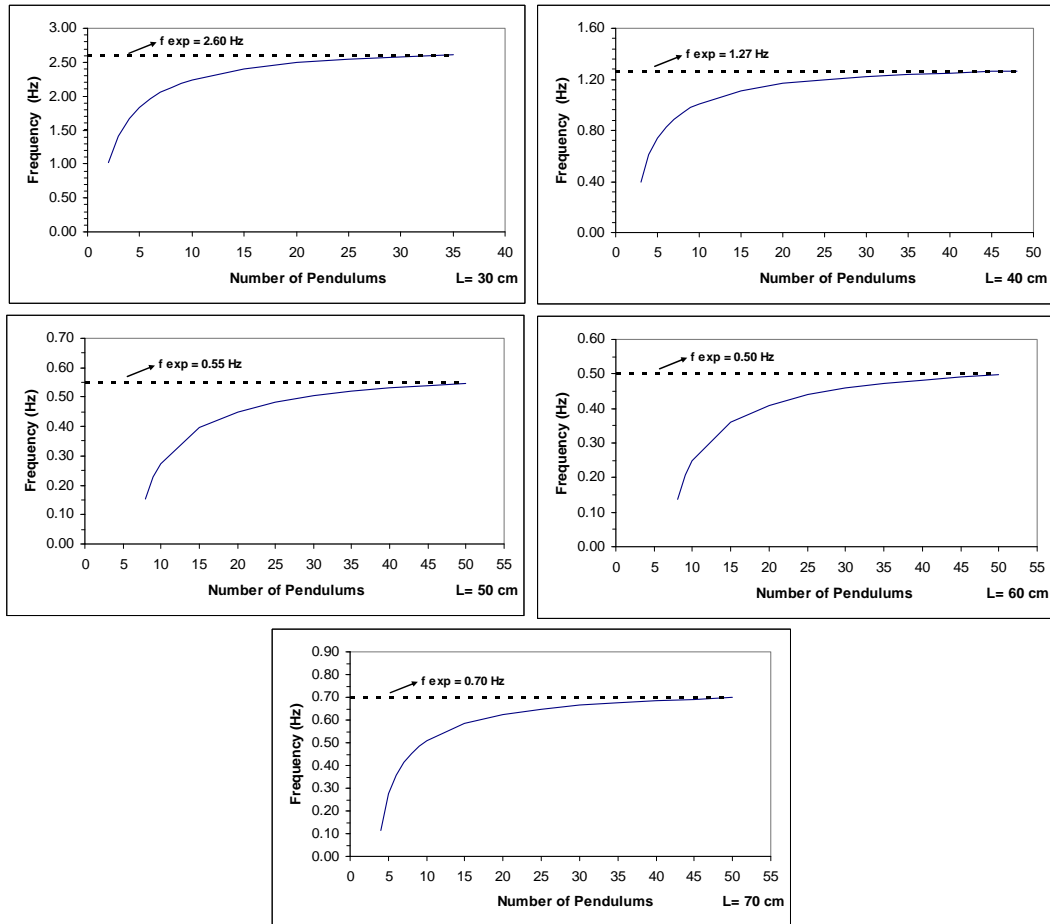


Fig. 3 Variation of the lowest natural frequency as a function of the number of pendulums

$$RM\ddot{\theta} + [RW + RK]\theta = 0 \tag{17}$$

As can be seen in Fig. 3, as the number of pendulums increase the frequency approaches asymptotically from below the experimental results for all values of L , including the cases when and $L > L_{cr}$.

Fig. 4 shows the critical load of the slender column as a function of the number of pendulums, obtained from the eigenvalue problem

$$[RW + RK]\theta = 0 \tag{18}$$

Again, as the number of pendulums increase, the critical load approaches asymptotically from below the theoretical value, $q_{cr} = 1.9374$, obtained by Gonçalves *et al.* (2006). A number of pendulums equal to 50 is enough to describe the lowest natural frequency and critical load accurately. So, this discretization is used in the following parametric analysis.

Fig. 5 shows the variation of the lowest natural frequency as a function of the column length for a beam under compression (Fig. 5(a)) and tension (Fig. 5(b)). In both cases the natural frequency

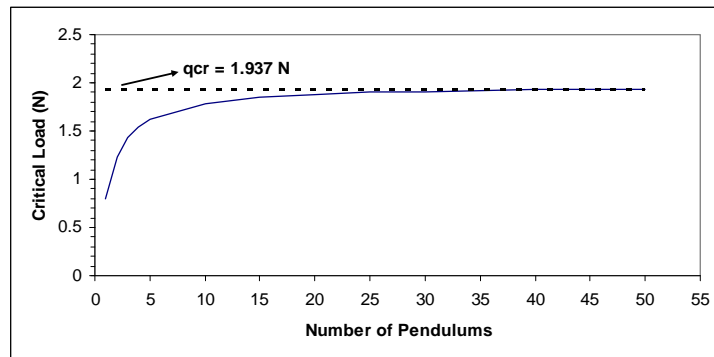


Fig. 4 Critical load as a function of the number of pendulums

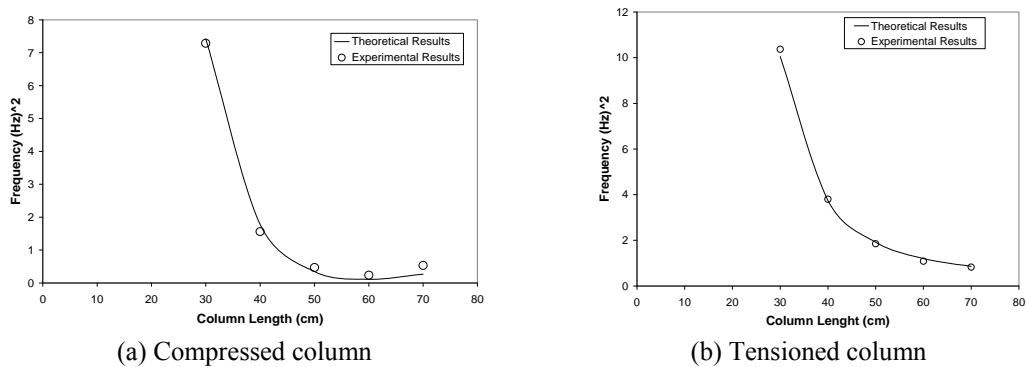


Fig. 5 Variation of the square of the lowest experimental and theoretical natural frequency as a function of the length L for the compressed column (a) and tensioned column (b)

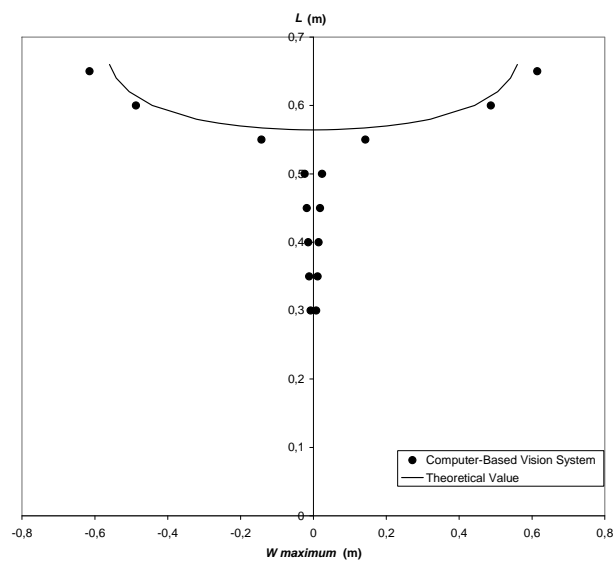


Fig. 6 Post-buckling path of a clamped-free column – Comparison between numerical and experimental (Computer-Based Vision System) results

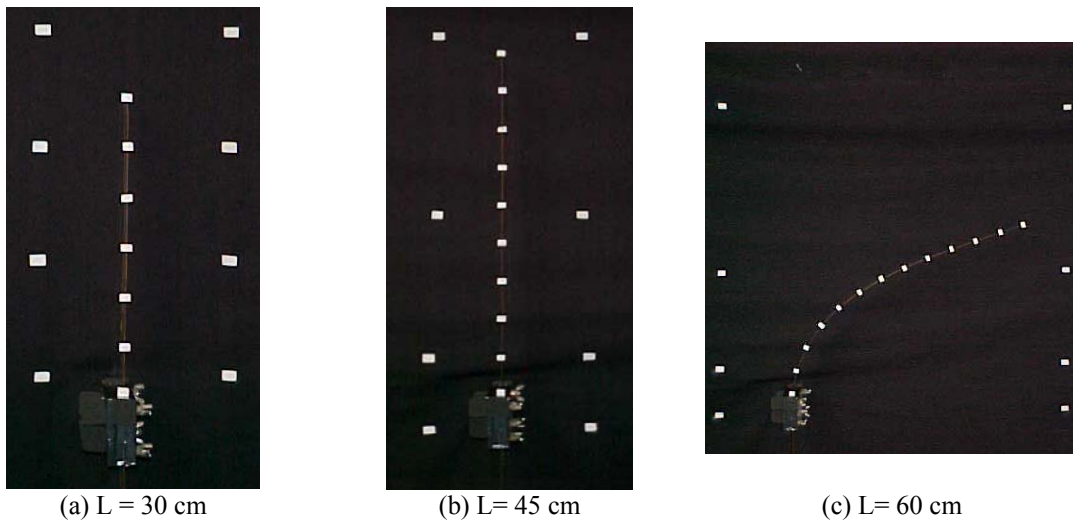


Fig. 7 Clamped-free slender metal columns – Images from Computer-Based Vision System (Image Sensor Program – ISP)

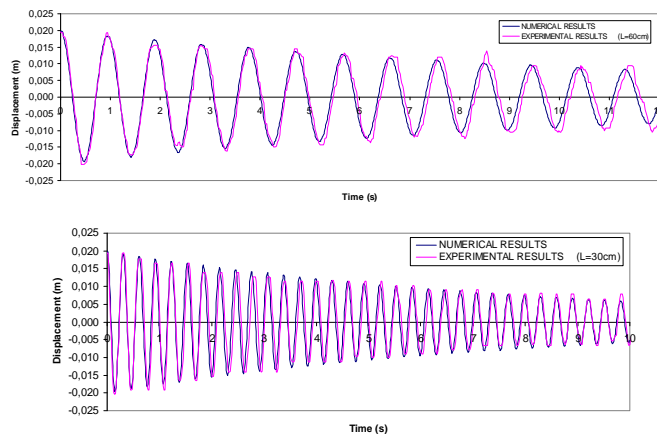


Fig. 8 Comparison between the numerical and experimental dynamic responses for tensioned columns (column modeled with 35 pendulums)

decreases as the column length increases and excellent agreement is obtained between the theoretical and experimental results. For the compressed column, the natural frequency approaches zero as the length approaches the critical value and then increases slightly along the post-buckling path due to the small increase in the flexural stiffness.

Fig. 6 compares favorably the deflection of the tip of the compressed column obtained experimentally with the theoretical post-buckling path up to very large deflection. The final configuration for selected values of L is shown in Fig. 7. The small difference around the stable pitchfork bifurcation is due to small imperfections. This is expected, since the pitchfork bifurcation is from a mathematical point of view structurally unstable. These results confirm the accuracy of the mathematical model for this problem.

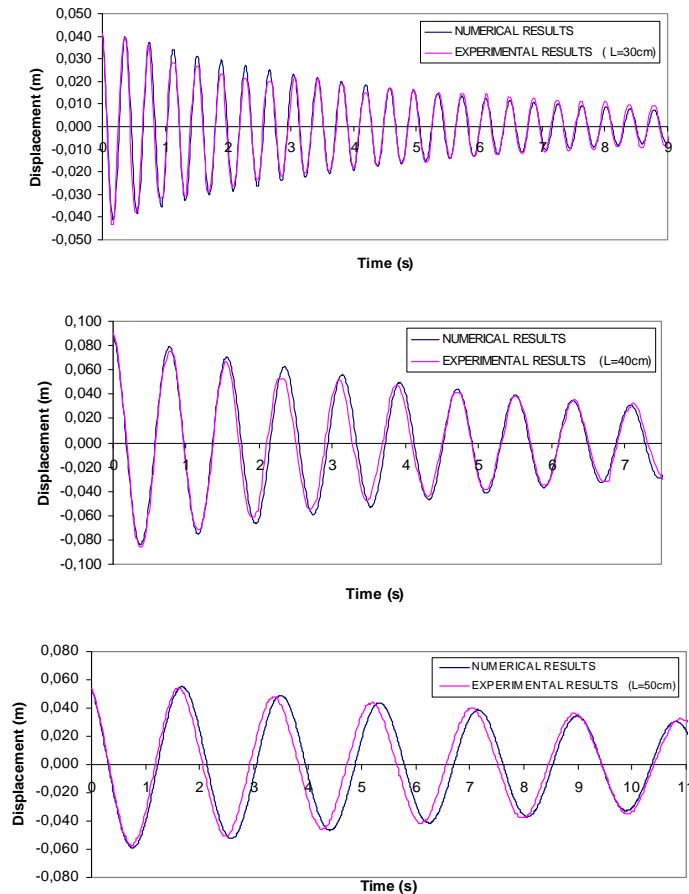


Fig. 9 Comparison between the dynamic responses obtained by the numerical modeling and by the ISP for $L < L_{cr}$

Fig. 8 shows the variation of the displacement at the tip of the column obtained by numerical integration of the equations of motion and the results obtained experimentally, using the ISP, for different column lengths under tension, while Fig. 9 shows the same comparison for the compressed column for $L < L_{cr}$. In both cases the results show excellent agreement between theoretical and experimental results during the nonlinear transient response. The damping coefficient used in the theoretical model was obtained from the experimental analysis.

Fig. 10 shows the comparison between numerical and experimental results for $L > L_{cr}$. In such cases, the column vibrates around the stable post-buckling position, exhibiting large deflections due to the small post-buckling stiffness.

To verify the influence of small geometric imperfections on the oscillation of the column, the initial column profile was obtained using the computer-based vision system and included in the theoretical model. Fig. 11 shows the comparison of the experimental time response with the numerical response considering or not the initial imperfections. The results show that the initial imperfections in the experimental model have negligible effect on the results.

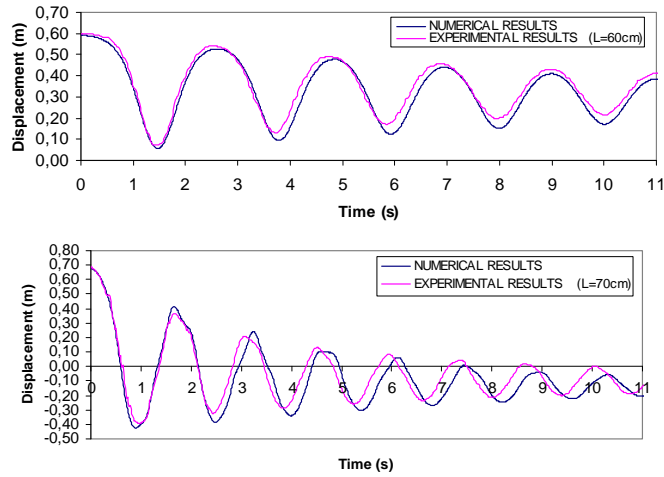


Fig. 10 Comparison between the dynamic responses obtained by the numerical modeling and by the ISP for $L > L_{cr}$

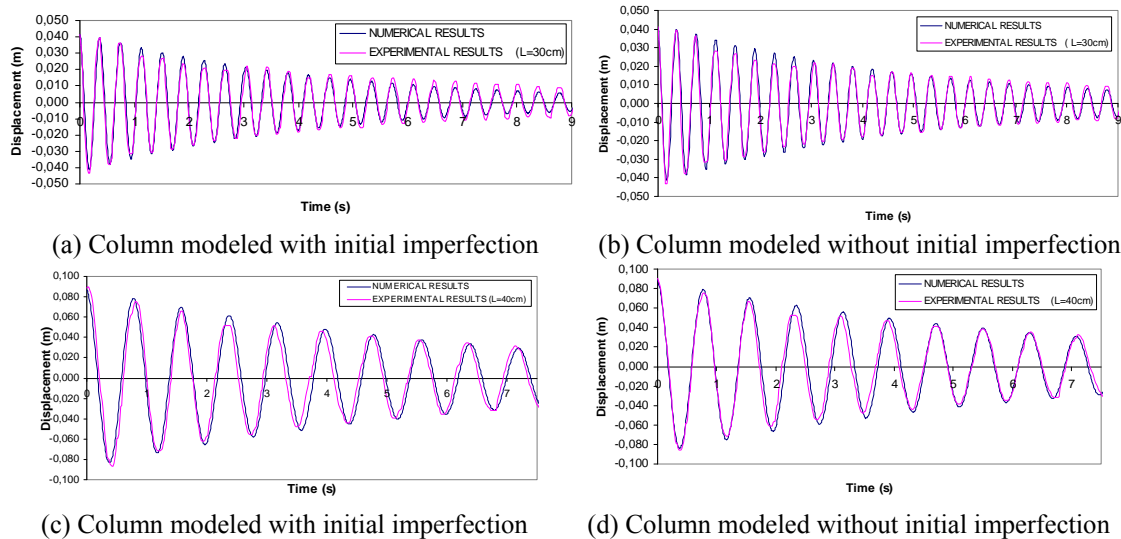


Fig. 11 Comparison between the dynamic responses obtained by the numerical modeling, taking into account (and not taking) initial imperfection, and by the ISP for columns with $L < L_{cr}$

Due to the inherent geometrical and inertial nonlinearities of the problem, the vibration frequency varies with the vibration amplitude leading to a nonlinear frequency-amplitude relation. The frequency-amplitude relation is obtained here from the theoretical and experimental time response using the methodology proposed by Nandakumar and Chatterjee (2005) as follows: the time response of the damped system is obtained and the maximum amplitude and corresponding period between two consecutive positive peaks are computed at each cycle. Consider two successive peaks at times T_1 and T_2 . Let their average value be A_1 . Let the trough between these two positive peaks be A_2 . We then define the amplitude as $A = (A_1 - A_2)/2$, and the frequency as $\omega = 1/(T_1 - T_2)$. The resulting amplitude and frequency values are plotted to give the nonlinear

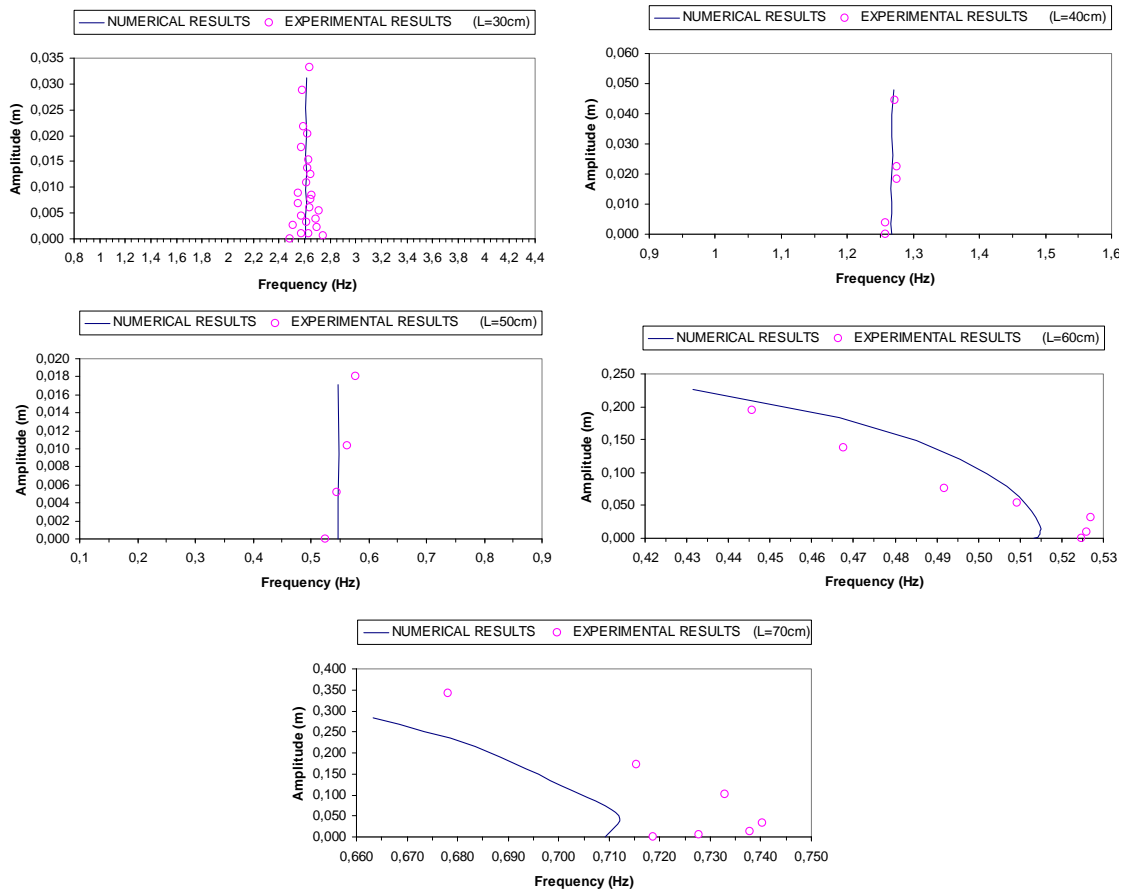
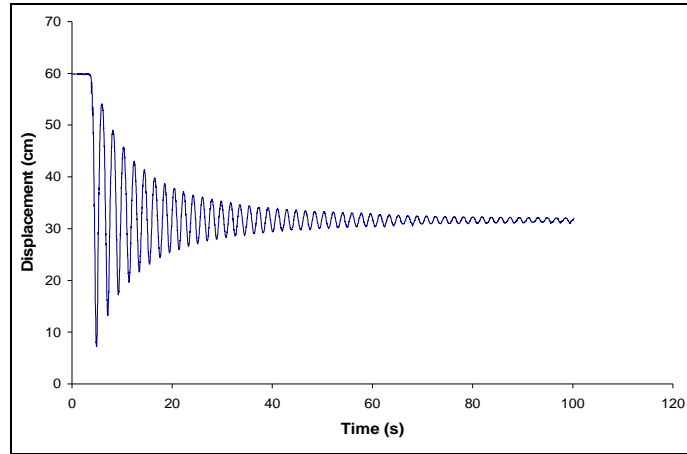


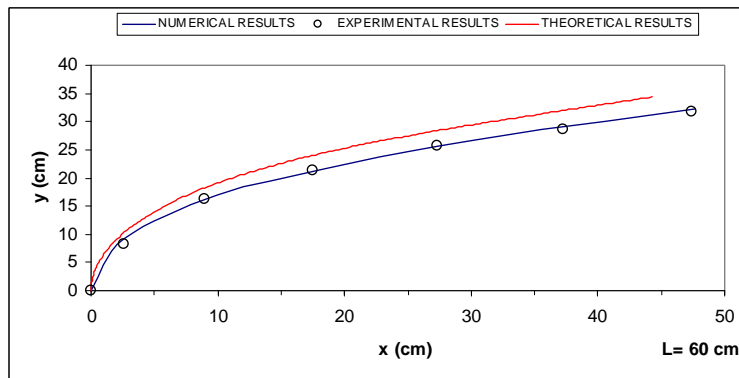
Fig. 12 Natural frequency behavior as a function of the free-vibration movement amplitude

frequency-amplitude relation. Fig. 12 shows the variation of the “instantaneous frequency” as a function of time for increasing values of the column length. For $L < L_{cr}$ the response is practically linear, while for $L > L_{cr}$ the column exhibits a characteristic softening behavior. This behavior of the natural frequency is related to the loss of stiffness due to the influence of the self-weight together with large rotations which are inherent to the free vibrations of columns with a high slenderness ratio. Recently, Chirikov (2003) also observed a *softening phenomenon* in the vibration analysis of beams undergoing large rotations. Nayfeh and Pai (2004) discuss the relative importance of the geometric and inertial nonlinearities on the softening behavior of slender beams. For the case of the tensioned column, practically no variation of the natural frequency with vibration amplitude is observed in the experimental results during the damped free-vibration response.

When the column length is much higher than the critical value and it is released from an unstable post-buckling position, thus exhibiting large deflections, most formulations are unable to describe the strong variation of displacements and velocities during the divergence process. However the present formulation is capable of describing with accuracy such highly nonlinear process. Figs. 13 and 14 show for the columns with $L=60\text{cm}$ and $L=70\text{cm}$, respectively, the time

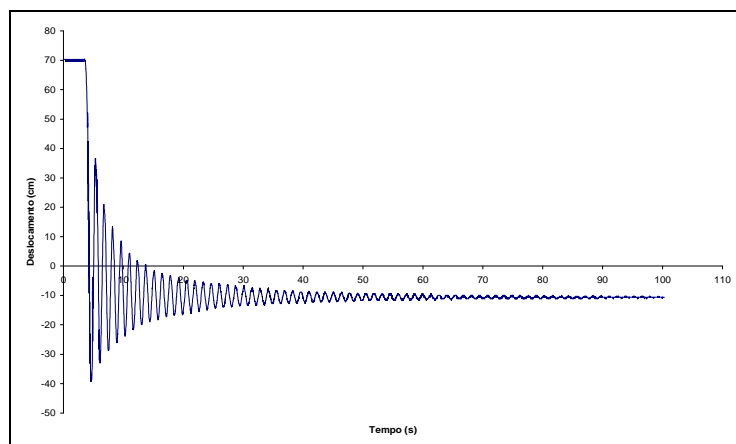


(a) Dynamic response



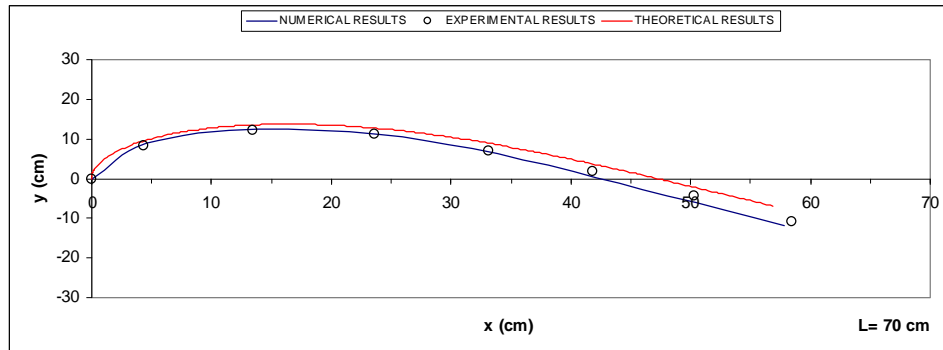
(b) Deformed shapes

Fig. 13 Comparison of the experimentally obtained deformed shapes with the numerical and theoretical results for slender column with $L=60\text{cm}$ ($L>L_{cr}$)



(a) Dynamic response

Fig. 14 Comparison of the experimentally obtained deformed shapes with the numerical and theoretical results for slender column with $L=70\text{cm}$ ($L>L_{cr}$)



(b) Deformed shapes

Fig. 14 Continued

response together with the final stable post-buckling configuration. In these figures the theoretical result (red curve) is the solution obtained by direct integration of the fully nonlinear equilibrium equations of the continuous system by the shooting method (Gonçalves *et al.* 2006).

5. Conclusions

The proposed experimental methodology has proved to be an efficient tool for a precise nonlinear dynamic analysis of structures that cannot be monitored by conventional sensors. One of the advantages of the developed computational vision system is the capacity to measure dynamic displacements in several points of the structure with efficiency and accuracy, allowing in this way a better identification of the structural behavior. Another advantage is related to the low cost of the developed measurement system, as compared to conventional systems. The proposed mathematical modeling for the slender column as a system of n coupled pendulums connected by damped rotational springs can capture in an accurate form all geometric and inertial nonlinearities due to large deflections and rotations. Moreover, the excellent comparison between numerical and experimental results shows that, as the number of pendulums increase, the model behavior approaches that of a continuously flexible beam. The parametric analysis considering an increasing column length clarifies the influence of self-weight on the nonlinear oscillations of the column in the pre- and post-buckling ranges. While tensioned or compressed bars with length lower than the critical one display a small degree of nonlinearity, compressed bars in the post-buckling regime exhibit a nonlinear softening frequency-amplitude relation due to the effect of large rotations.

Acknowledgments

The authors wish to thank the Brazilian research agencies CNPq, CAPES and FAPERJ and the National Petroleum Agency (ANP) for their financial support.

References

- Abdel-Aziz, Y.I. and Karara, H.M. (1971), "Direct linear transformation from comparator coordinates into object space coordinates in close-range photogrammetry", *Proceedings of the Symposium on Close-Range Photogrammetry, Falls Church, VA: American Society of Photogrammetry*, 1-18.
- Braun, M. (2003), "On some properties of the multiple pendulum", *Archive of Applied Mechanics*, **72**, 899-910.
- Chen, L., Armstrong, C.W. and Raftopoulos, D.D. (1994), "An investigation on the accuracy of three-dimensional space reconstruction using the direct linear transformation technique", *J. Biomechanics*, **27**, 493-500.
- Chirikov, V.A. (2005), "Causes for the softening phenomenon at vibrations of beams undergoing large rotation", *ENOC-2005, Eindhoven, Netherlands*, 2541-2547.
- Duan, W.H. and Wang, C.M. (2008), "Exact solution for buckling of columns including self-weight", *Journal of Engineering Mechanics, ASCE*, **134**(1), 116-120.
- Faugeras, O.D. and Toscani, G. (1986), "The calibration problem for stereo", *Proceedings of the IEEE Computer vision and Pattern Recognition*.
- Galán, J., Fraser, W.B., Acheson, D.J. and Champneys, A.R. (2005), "The parametrically excited upside-down rod: an elastic jointed pendulum model", *Journal of Sound and Vibration*, **280**, 359-377.
- Gonçalves, P.B., Jurjo, D.L.B.R., Magluta, C., Roitman, N. and Pamplona, D. (2006), "Large deflection behavior and stability of slender bars under self-weight", *Structural Engineering and Mechanics*, **24**, 709-725.
- Haralick, R.M. and Shapiro, L.G. (1993), *Computer and Robot Vision 2*, Addison-Wesley Publishing Company, NY.
- Hack, E. and Leroy, D. (2005), "Camera-based monitoring of the rigid-body displacement of a mandrel in superconducting cable production", *Optics and Lasers in Engineering*, **43**, 455-474.
- Hatze, H. (1988), "High-precision three-dimensional photogrammetric calibration and object space reconstruction using a modified DLT-approach", *J. Biomechanics*, **21**, 533-538.
- Ito, M. (1991). "Robot vision modeling, camera modeling and camera calibration", *Adv. Robotics*, **5**, 321-335.
- Jones, A., Shaw, J. and Wineman, A. (2006), "An experimental facility to measure the chemorheological response of inflated elastomeric membranes at high temperature", *Experimental Mechanics*, **46**, 579-587.
- Jurjo, D.L.B.R. (2007), "Development of a computer-based vision system for measuring displacements in structures", PhD. Thesis, Civil Engineering Department, COPPE/UFRJ, Brazil. (in Portuguese)
- Jurjo, D.L.B.R., Magluta, C., Roitman, N. and Gonçalves, P.B. (2010), "Experimental methodology for the dynamic analysis of slender structures based on digital image processing techniques", *Mechanical Systems & Signal Processing*, **24**, 1369-1382.
- Lee, J.J. and Shinozuka, M. (2006a), "Real-time displacement measurement of a flexible bridge using digital image processing techniques", *Experimental Mechanics*, **46**, 105-144.
- Lee, J.J. and Shinozuka, M. (2006b), "A vision-based system for remote sensing of bridge displacement", *NDT & E International*, **39**, 425-431.
- Nandakumar, K. and Chatterjee, A. (2005), "Resonance, parameter estimation, and modal interactions in a strongly nonlinear benchmark oscillator", *Nonlinear Dynamics*, **40**, 149-167.
- Nayfeh, A.H. and Pai, P.F. (2004), *Linear and Nonlinear Structural Mechanics*, Wiley, New York.
- Neukirch, S., Frelat, J., Goriely, A. and Maurini, C. (2012), "Vibrations of post-buckled rods: The singular inextensible limit", *Journal of Sound and Vibration*, **331**, 704-720.
- Sadiku, S. (2008), "Buckling load optimization for heavy elastic columns: a perturbation approach", *Structural and Multidisciplinary Optimization*, **35**(5), 447-452.
- Santillan, S.T., Plaut, R.H., Witelski, T.P. and Virgin, L.N. (2008), "Large amplitude oscillations of beams and columns including self-weight", *International Journal of Nonlinear Mechanics*, **43**, 761-771.
- Sathyamoorthy, M. (1998), *Nonlinear Analysis of Structures*, CRC Press, New York.

- Tolou, N. and Herder, J.L. (2009), "A semianalytical approach to large deflections in compliant beams under point load", *Mathematical Problems in Engineering*, 910896.
- Tsai, R.Y. (1986), "An efficient and accurate camera calibration technique for 3D machine vision", *Proceedings of IEEE Conference on Computer Vision and Pattern Recognition*, Miami Beach, FL.
- Vaz, M.A. and Mascaro, G.H.W. (2005), "Post-buckling analysis of slender vertical rods subjected to terminal forces and self-weight", *Int. J. Non-linear Mechanics*, **40**, 1049-1056.
- Virgin, L.N. and Plaut, R.H. (2004), "Postbuckling and vibration of linearly elastic and softening columns under self-weight", *Int. J. Solids Struct.*, **41**, 4989-5001.
- Wang, C.Y. (2010), "Vibration of a segmented heavy column", *J. Vib. Acoust.*, **132**(2), 4.
- Wei, D.J., Yan, S.X., Zhang, Z.P. and Li, X.F. (2010), "Critical load for buckling of non-prismatic columns under self-weight and tip force", *Mechanics Research Communications*, **37** (6), 554-558.
- Weng, J., Cohen, P. and Herniou, M. (1992), "Camera calibration with distortion models and accuracy evaluation", *IEEE Trans. Pattern Anal. Mach. Intell.*, **14**, 965-980.
- Yoneyama, S., Morimoto, Y., Fujigaki, M. and Ikeda, Y. (2005), "Scanning Moiré and spatial-offset phase-stepping for surface inspection of structures", *Optics and Lasers in Engineering*, **43**, 659-670.